

# Simulated expansion of an ultra-cold, neutral plasma

F. Robicheaux<sup>a)</sup> and James D. Hanson

*Department of Physics, Auburn University, Alabama 36849-5311*

(Received 3 February 2003; accepted 17 March 2003)

The details of recent calculations of the expansion of ultra-cold, neutral plasmas are given. The calculations are performed at several levels. The simplest level assumes an ansatz for the form of the electron and ion density; the result is a simple, ordinary differential equation which can be easily solved. The medium level of sophistication assumes the electrons are in thermal equilibrium but does not assume a particular form for the ion density; the result is a partial differential equation which is solved numerically. For the highest level of sophistication, a Monte Carlo technique is used to solve for the electron phase space distribution and solve for the ion motion in the resulting mean field. All levels of simulation include three body recombination and electron-Rydberg scattering. This paper contains the results of our simulations and compares them to measurements made on ultra-cold plasmas. Three body recombination is found to be important at very low temperatures since it is a heating mechanism for the electron gas. The collisions between cold electrons and Rydberg atoms are another important source of electron heating and de-excitation of atoms formed in the plasma. The evolution of the distribution of atoms in the plasma is simulated and several counter-intuitive effects that have been observed can be explained. Our simulations show that the plasma coupling constant does not become larger than  $\sim 1/5$  for the reported experiments. The behavior of plasma processes are investigated, e.g., ion acoustic waves, spike formation, and electron evaporation. The evolution of a cold Rydberg gas into a plasma is also simulated but certain properties of our simulation do not agree with measurements. © 2003 American Institute of Physics. [DOI: 10.1063/1.1573213]

## I. INTRODUCTION

The ability to cool and trap atomic gases is one of the interesting experimental advances of the past 20 years.<sup>1</sup> These techniques have been used to create Bose–Einstein condensates of simple atomic gases, degenerate Fermi gases, advances in atomic clocks, and many other systems. There are several different methods that use light to cool atoms. In an optical molasses, 6 lasers (2 counterpropagating beams on 3 orthogonal axes) are tuned to a lower energy than an atomic transition. A moving atom experiences a resistive force because the Doppler effect gives larger photon absorption from the light with momentum opposite to that of the atom; the atom later re-emits the photon in a random direction thus giving a net momentum decrease to the atom. This technique can reduce the energy of the atom to roughly  $\hbar$  times the frequency width of the transition. In a magneto-optical trap, the atoms can be cooled below 1 mK by using an inhomogeneous magnetic field and simple diode lasers. A magnetic field splits the energy levels of an atom and this splitting is proportional to the field strength for a small magnetic field. The lasers are detuned (and polarized) so the atoms tend to absorb photons from the beam that pushes them back to the center of the trap. The density of atoms can be as high as  $\sim 10^{11} \text{ cm}^{-3}$ .

Several groups have used the cold atoms from magneto-optical traps as the starting point for the investigation of ultra-cold plasmas.<sup>2–8</sup> In one type of experiment, atoms are

cooled to less than a mK and are then photo-ionized by a laser. The free electrons escape the region of the positive ions until a large enough space charge develops to bind the remaining electrons. The initial size of the plasma is a few hundred microns. The initial energy of the electrons (which directly translates into an electron temperature,  $T_e$ ) can be controlled by tuning the laser frequency that ionizes the cold atoms and the number of electrons,  $N_e$ , and ions,  $N_i$  (and the corresponding densities  $n_e$  and  $n_i$ ) can be controlled through the laser intensity. Because the plasma is created by photo-ionizing cold atoms, the positive ions initially have the same temperature as the cold atoms; thus the positive ions initially have kinetic energy much less than the electrons. The electrons that are trapped by the space charge exert a thermal pressure which causes the plasma to expand. This expansion must result from the transfer of electron thermal energy and electrostatic energy of the mean electric field to radially directed kinetic energy of the ions. Thus, the electron part of the plasma cools and decreases in density with time.

Several of the plasma parameters are under direct control and are accurately known. Two of the parameters that typify a plasma are the Debye length which gives the distance over which a charge is screened and the Coulomb coupling parameter which is the ratio of the potential energy between adjacent charged particles to the kinetic energy. The expression for the Debye length is  $\lambda_D = \sqrt{\epsilon_0 k_B T_e / n e^2}$  while the Coulomb coupling parameter is  $\Gamma_e = (e^2 / 4\pi\epsilon_0 a) / k_B T_e$  where  $a = (3/4\pi n)^{1/3}$  is a typical distance between electrons. For a 50 K electron gas with a density of  $10^9 \text{ cm}^{-3}$ , these

<sup>a)</sup>Electronic mail: robicfj@auburn.edu

parameters have the values  $\lambda_D = 15 \mu\text{m}$  (which is  $\sim 20$  times smaller than the plasma),  $a = 6.2 \mu\text{m}$ , and  $\Gamma = 0.054$ . The Coulomb coupling parameter is especially important because if it is roughly 1 or larger then the potential energy dominates and highly correlated motion between charged particles is expected. The experiments can tune the plasma so that  $\Gamma_e \gg 1$ . It is precisely when the Coulomb coupling parameter was roughly equal to or greater than 1 that some of the strange results in Refs. 3 and 4 were obtained.

For many of the ultra-cold plasmas, atomic processes play a major role the dynamics. Electrons can scatter in the field of a positive ion so that one electron loses enough energy to become bound to the ion with the other electron gaining energy. This process is known as three body recombination. The recombination rate decreases as the electron density decreases but increases as the electron temperature decreases:  $A_{\text{TBR}} \propto n_e^2 T_e^{-9/2}$ .<sup>9</sup> For ultra-cold plasmas, a substantial number of three body recombination events can occur. The atoms formed through three body recombination have binding energy of roughly  $2k_B T_e$ . At low temperatures, the atoms are very highly excited and are known as Rydberg atoms. The electrons in the plasma can scatter from these atoms and gain energy which means the Rydberg atoms are a source of heat for the electrons. Another important consideration is that the radius of the atom formed in three body recombination divided by the distance between ions is roughly  $\Gamma_e/2$ ; this means that the basic process of three body recombination needs to be revisited if the Coulomb coupling parameter becomes larger than 1. The ultra-cold plasmas are interesting because atomic physics processes strongly affect the behavior of the plasma and because of the level of experimental control of plasma parameters.

In the experiments performed at the National Institute of Standards and Technology (NIST),<sup>2-4</sup> atoms are cooled to  $\mu\text{K}$  temperatures before being photo-ionized. In the first experiment,<sup>2</sup> the time dependence of the rate that electrons leave the plasma could be measured. There is a prompt "burst" of electrons that leave the plasma (to within  $1 \mu\text{s}$  of the laser pulse) until a sufficient space charge develops to bind the remaining electrons; the fraction of electrons that leave in the prompt burst was explained and depends on several of the plasma parameters: electron temperature ( $T_e$ ), number of electrons ( $N_e$ ), and size of the plasma. In the second experiment,<sup>3</sup> the time dependence of the electron density was measured between roughly 1 and  $100 \mu\text{s}$ . The plasma expands because the thermal pressure from the electrons exerts a radially outward force on the ions. The asymptotic expansion velocity is simply a result of the conservation of energy (thermal energy of the electrons is converted to radial kinetic energy of the ions) and does not depend on detailed calculations. However, the ions were measured to expand too fast at the lowest temperatures which indicates that an additional source of energy was present. In the third experiment,<sup>4</sup> the energy source for the anomalous plasma expansion was identified: a substantial number of Rydberg atoms were present in the plasma. The Rydberg atoms must arise from recombination and for every recombination extra energy is given to the remaining elec-

trons. However, several properties of the Rydberg atoms did not agree with ideas for any recombination mechanism (e.g., three body recombination); thus, the recombination mechanism was an open question.

In a second type of experiment, very cold atoms are excited into Rydberg states. These highly excited atoms can be (relatively) easily stripped of an electron. Under certain conditions, the gas of Rydberg atoms converts into an ultra-cold plasma. The conversion takes place over a few microseconds in many cases. Several properties of the atoms in the plasma have been measured. The physical process that causes the Rydberg gas to convert to a plasma is not known.

In experiments performed at Virginia and Aime Cotton,<sup>5</sup> Connecticut,<sup>6</sup> and Michigan,<sup>7</sup> atoms were cooled to  $\mu\text{K}$  temperatures before being excited into Rydberg states. The cold Rydberg atoms evolve into a plasma<sup>5</sup> which later evolves back into a Rydberg gas.<sup>6</sup> In Ref. 5, the mechanism for the Rydberg gas to evolve into a plasma has not been determined; in particular, the source of the energy required to convert a gas of Rydberg atoms into a plasma has not been identified. In Ref. 6, the Rydberg gas transforms into a plasma too rapidly for the parameters of their experiment; the mechanism for the Rydberg gas to plasma conversion has only been speculated upon. In experiments performed at Michigan,<sup>7</sup> a cold Rydberg gas was produced; the Rydberg gas had a lifetime much longer than expected due to  $l$ -changing collisions of the gas with free electrons.

Four groups<sup>10-14</sup> have independently simulated some aspects of the experiments that directly create free electrons. In Refs. 11, 13, and 14, full molecular dynamics simulation of the electron and ion motion was able to follow the plasma dynamics for the very early stages of the plasma expansion ( $\ll 1 \mu\text{s}$ ). In these simulations, it was clear that three body recombination rapidly heated the free electrons when the initial electron temperature was below  $\sim 10-20 \text{ K}$ . These simulations showed that three body recombination was important at early times but did not address the evolution of the plasma and the recombination mechanism during the main part of the plasma expansion. The simulations in Ref. 10 used ideas of a "metastable plasma" to simulate aspects of ultra-cold plasmas.

Our previous simulations in Ref. 12 were completely different in character. In our simulations, the plasma was assumed to be weakly coupled and we solved for the plasma dynamics including the mean field, a Monte Carlo treatment of two body collisions, and a rate equations for three body recombination. Simulations were performed at several levels of sophistication. Because of the approximations in our simulations compared to the molecular dynamics treatments,<sup>11,13,14</sup> we were able to follow the plasma for the duration of the experiments. In our simulations, the Coulomb coupling parameter would stay much less than 1 (or rapidly drop to values much less than 1) which means our simulations were self consistent. We found that we could describe many of the nonintuitive features measured in Refs. 3,4 and could predict some properties of ultra-cold plasmas that have not been measured yet.

Our purpose in this paper is to present the details of our simulations and to present some new results relating to ultra-

cold plasmas. Some of the new results relate to the details of the electrons evaporating from the plasma, to ion acoustic waves in ultra-cold plasmas, and to the distribution of Rydberg atoms formed in the plasma. We also give some of the details showing the agreement between different degrees of approximation. We also present results of the first simulation of a cold Rydberg gas converting to an ultra-cold plasma; our simulations showed many similarities to the measurements but were ultimately in disagreement with a main component of the experiment.

## II. ION SIMULATION

All of our simulations treat the ions as a zero pressure fluid. Thus, we start by examining our treatment of the ions and the accuracy of this approximation.

The ions start at a very low temperature in the ultra-cold plasma; for all initial conditions in published experiments, the initial ion temperature is much lower than the electron temperature. Given enough time the electrons and ions would come into thermal equilibrium. However, the main action in most of the experiments occurs in the earliest 10's of  $\mu\text{s}$  after creation of the plasma. The ions hardly heat up over this short a time. The time required for the electrons and ions to come into thermal equilibrium is roughly the time for the electrons to come into thermal equilibrium with themselves times the ratio of the ion mass to the electron mass,  $M_i/M_e \sim 2.5 \times 10^5$ . Thus, the time required for the ions to gain *thermal* energy is much longer ( $\sim 10^{-3}$  s) than the time over which the interesting plasma dynamics occurs.

In our simulations, we use an equally spaced radial grid (spacing  $\delta r$ ) for computing ion and electron densities,  $n_i(r)$  and  $n_e(r)$ , and from these densities we compute mean electric fields and potentials; the radial grid extended to  $40 \times$  the size of the plasma with 12,000 radial points. We represent the  $N_i$  ions using  $\tilde{N}_i$  particles that move in the mean fields according to Newton's equation. Each particle has a weight  $w_i = N_i/\tilde{N}_i$  and contributes to the weighted density,  $r^2 n_i(r)$ , through a tent function that covers 8 radial grid points. The weight that each particle contributes to the density depends on the actual number of ions being simulated, the number of particles used to treat the ion motion, and how much recombination has occurred for the particle as described in Sec. IV.

The initial distribution of particles is chosen to give the correct ion density at the initial time. The velocity of all of the particles is chosen to be zero initially. The acceleration,  $a_j$ , of ion  $j$  at radial position  $r_j$  is computed by interpolating the function  $r^2 a(r)$  to the position of the particle using the two radial grid points that bracket the particle and dividing the interpolated value by  $r_j^2$ . The function  $r^2 a(r)$  is proportional to the total charge density inside the sphere of radius  $r$  which is smoother than the acceleration,  $a(r)$ . But more importantly, this interpolation ensures that the ion self-force behaves appropriately and does not introduce spurious forces and energy into the simulation.

Although we expect our simulation of ion motion to work well for all cases treated in this paper, we note that treating the ions as a zero pressure fluid prevents us from

simulating phenomena discussed in Refs. 13–15 relating to the formation of strongly coupled ion motion.

## III. ELECTRON SIMULATION

The electrons have much larger acceleration than the ions because of the enormous ratio of ion to electron mass. Thus, simulating the electron motion is computationally intensive. We resorted to approximate treatments of electron motion in order to reach the long times of the experiments.

### A. Particle model

In our most sophisticated simulations, we use Monte Carlo ideas to simulate the electron motion. The electron density is simulated using  $\tilde{N}_e$  particles to represent the  $N_e$  electrons in the plasma. Each of the particles has a statistical weight  $w_e = N_e/\tilde{N}_e$ . The electric forces on the electrons can be divided into a mean field force from the ions and all other electrons and a rapidly fluctuating force due to short range collisions between pairs of electrons and between electrons and ions. The mean field force is treated by propagating the electrons using Newton's equations with the acceleration being  $-\vec{E} \cdot e/M_e$ . We treat the collisions (which causes the electron distribution to approach thermal equilibrium) using a Monte Carlo technique. The particles are evolved in three spatial dimensions but the computations assume the mean density has spherical symmetry.

Since the ions and the electrons have a spherical distribution inside the plasma, the radial component of the mean electric field is computed from

$$E_r(r) = \frac{e}{\epsilon_0 r^2} \int_0^r dr r^2 [n_i(\bar{r}) - n_e(\bar{r})], \quad (1)$$

where the ion density,  $n_i$ , is calculated as described above. The radial electric field is computed on a grid of equally spaced radial points: the  $j$ -th grid point is  $r_j = j \cdot \delta r$ . The weighted electron density,  $n_e \cdot 4\pi r^2 \delta r$ , is computed from the positions of the electron particles using a tent function covering two radial grid points; we did not need the tent function to cover many grid points because the electrons rapidly moved through different radial regions which provided an averaging not present for the ions. The tent function is chosen to exactly conserve the charge and to prevent the electron from acting back on itself which could have disastrous effects on energy conservation.

We note that the mean field in our simulation fluctuates because the electrons move rapidly through the plasma and the number of particles between successive grid points is not large. Also, the radial electric field depends on the difference between the ion and electron densities which are very similar at low temperatures. Since the difference in density is much smaller than the densities, the fluctuations in the mean field are proportionately larger; the fluctuation is largest at small  $r$  since this has the smallest volume and thus the smallest number of particles. We ensured that the fluctuations did not affect our result by increasing the number of particles until the results stabilized.

We accounted for the electron–ion collisions and the electron–electron collisions using a Monte Carlo treatment. The electron–ion collisions cause the direction of the electron’s velocity to change in random manner. The electron–electron collisions cause the direction of the relative velocity vector between two electrons,  $\vec{v}_1 - \vec{v}_2$ , to change in a random manner; these collisions cause the electron distribution to trend to a thermal distribution. We give a detailed derivation of our treatment of the electron–ion collisions.

It is well known that the direction of the electron’s velocity changes randomly during a short time interval  $\delta t$  due to collisions with ions. The expectation value of the squared change in direction is<sup>16</sup>

$$\langle \Delta \theta^2 \rangle \approx n_i v_e \delta t \frac{e^4}{2 \pi \epsilon_0^2 M_e^2 v_e^4} \ln \Lambda, \tag{2}$$

where  $\Lambda$  is (roughly speaking) the ratio of the maximum impact parameter to the minimum impact parameter in a collision; since  $\Lambda$  is inside the logarithm usually the exact value is not important. By convention,  $\Lambda = 3k_B T_e / [e^2 / 4 \pi \epsilon_0 \lambda_D]$  where  $k_B$  is Boltzmann’s constant and  $\lambda_D = \sqrt{k_B T_e \epsilon_0 / e^2 n_e}$  is the Debye length.

The electron’s velocity changes direction due to Coulomb scattering and we simulate it by defining a differential cross section for electron–ion scattering that gives the same  $\langle \Delta \theta^2 \rangle$  as the usual treatment. We chose the form

$$\frac{d\sigma}{d\cos\theta} = \frac{e^4}{8 \pi \epsilon_0^2 M_e^2 v_e^4 [1 - \cos\theta + \Delta]^2}, \tag{3}$$

which gives the familiar Coulomb cross section for small impact parameter (large angle) scattering but cuts off the large impact parameter (small angle) scattering; the large impact parameter scattering is suppressed due to the screening from other electrons in the plasma. Other forms for the cross section were tried; our results were independent of the form of our cross section as long as  $\langle \Delta \theta^2 \rangle$  and the large angle form of the cross section were unchanged.

There is only one adjustable parameter in this form for the differential cross section,  $\Delta$ . We fix this to reproduce the usual expression for  $\langle \Delta \theta^2 \rangle$ :

$$\begin{aligned} \langle \Delta \theta^2 \rangle &= n_i v_e \delta t \int_{-1}^1 2(1 - \cos \theta) \frac{d\sigma}{d \cos \theta} d \cos \theta \\ &= n_i v_e \delta t \frac{e^4}{2 \pi \epsilon_0^2 M_e^2 v_e^4} \ln \sqrt{2/\Delta \exp(1)}, \end{aligned} \tag{4}$$

where  $\exp(1) = 2.718 \dots$ . It is clear from a comparison of Eqs. (2) and (4) that  $\Delta$  must have the value

$$\Delta = \frac{2}{\Lambda^2 \exp(1)}. \tag{5}$$

The electron–ion scattering is included in two steps. During a time interval  $\delta t$ , the probability for an electron scattering is

$$P = n_i v_e \delta t \sigma = n_i v_e \delta t \frac{e^4}{8 \pi \epsilon_0^2 M_e^2 v_e^4 \Delta}. \tag{6}$$

For an electron, a random number between 0 and 1 is generated and if the random number is less than  $P$  then a scattering event occurs. The angle through which the electron scatters is given by a second random number computed by using the differential cross section as a bias,

$$y = \int_{-1}^{\cos \theta} \frac{d\sigma}{\sigma d \cos \theta'} d \cos \theta', \tag{7}$$

where  $y$  is a random number with a flat distribution between 0 and 1. This equation can be inverted to give

$$\cos \theta = \frac{2(1 + \Delta)y - \Delta}{2y + \Delta}. \tag{8}$$

This gives the angle between the initial direction and the final direction. Finally, we rotate the final direction for the velocity around the initial direction by a random angle with a flat distribution between 0 and  $2\pi$ .

The electron–electron scattering is performed in a similar manner. Pairs of electron particles,  $j$  and  $k$ , are chosen so that the difference between the radial positions,  $|r_j - r_k|$ , is less than a small fraction of the plasma size (this criterion is varied until convergence is achieved); we choose pairs of particles whose radial distance from the plasma center differs by a small amount to obtain better statistics and because our simulations are for plasmas with spherical symmetry. If the particles are close enough to interact, the position of particle  $j$  is rotated to that of particle  $k$  and the velocity of particle  $j$  is rotated through the same angles. The inter-particle velocity,  $\vec{v}_- = \vec{v}_j - \vec{v}_k$ , is constructed along with the center of mass velocity  $\vec{v}_+ = (\vec{v}_j + \vec{v}_k)/2$ . The inter-particle velocity is then rotated similar to the prescription for electron–ion scattering except the reduced mass is used for electron–electron collisions. After the rotation of  $\vec{v}_-$ , the electrons’ velocities are reconstructed through

$$\vec{v}_j = \vec{v}_+ + \vec{v}_-/2, \quad \vec{v}_k = \vec{v}_+ - \vec{v}_-/2. \tag{9}$$

This treatment exactly conserves energy and gives the correct time dependence of the thermalization. After the scattering, the velocity and position of particle  $j$  is rotated back to its original position.

### 1. Results

At this level of approximation, we want to calculate how long it takes a region of the plasma to evolve to a Maxwell distribution, how long it takes different regions of the plasma to reach the same temperature, how many electrons leave the plasma at very early times, and how much energy is carried away by electrons at early times. The inputs to our simulation are the initial shape of the ion density, the number of free ions/electrons, and the initial energy of the electrons.

In Fig. 1, we plot the velocity distribution for electrons in a radial shell 1/4 out from the center of the plasma at three times. This shows how the velocity distribution approaches a

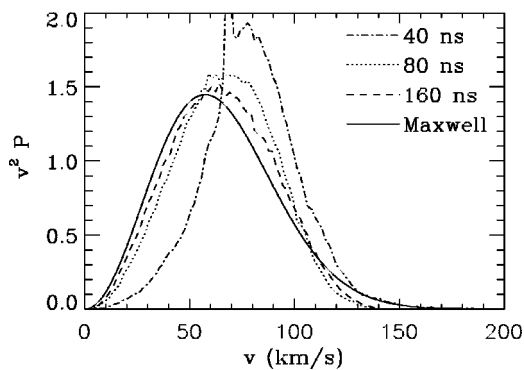


FIG. 1. The weighted velocity distribution 40 ns (dash-dotted line), 80 ns (dotted line), and 160 ns (dashed line) after the creation of the plasma compared to a Maxwell distribution (solid line); the electrons are chosen from a shell 1/4 out from the center of the plasma. The distribution at  $t = 0$  is a sharp spike at  $\sim 70$  km/s. The plasma has an initial average density, temperature, and  $\sqrt{\langle r^2 \rangle}$  of  $10^9$  cm $^{-3}$ , 100 K, and 340  $\mu$ m. The relaxation time is roughly 65 ns. We find that the actual distribution is very close to a Maxwell distribution by 400 ns and indistinguishable from a thermal distribution by 1000 ns.

local thermal distribution at roughly the time scale expected. Also as expected, the high energy tail of the distribution is populated more slowly.

However, the plasma as a whole takes much longer to reach thermal equilibrium. This can be seen in Fig. 2 where we show the temperature at different positions in the plasma. At each position, we use electrons within a small radial shell to obtain a temperature which is defined to be  $k_B T_e = (1/3) M_e \langle v^2 \rangle$ . Note that the center of the plasma becomes relatively hot while the edge of the plasma is relatively cool just after the plasma creation. Also at early times, the density of electrons at the center of the plasma is noticeably less than the proton density. The excess positive charge near the center of the plasma gives an extra acceleration of the electrons that enter this region. This accounts for the temperature spike at the center of the plasma at early times. Also, the higher energy electrons of the Maxwell distribution tend to be lost from the edge of the plasma but not from the center of the plasma. This tends to make the edge of the plasma cooler

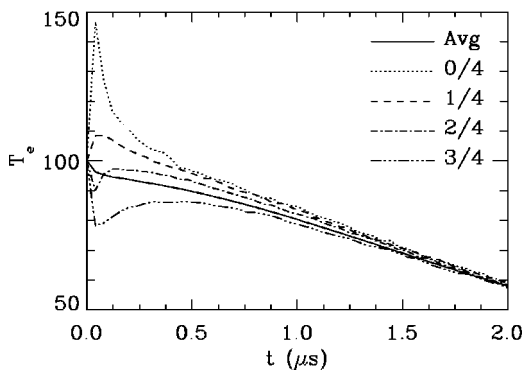


FIG. 2. The temperature at different radii in the plasma as a function of time for the same plasma parameters as Fig. 1. The positions are the following: center of the plasma (dotted line), 1/4 out from center (dashed line), 2/4 out from center (dash-dotted line), 3/4 out from center (dash-dot-dot-dot line). The average temperature for the innermost 80% of the electrons is the solid line.

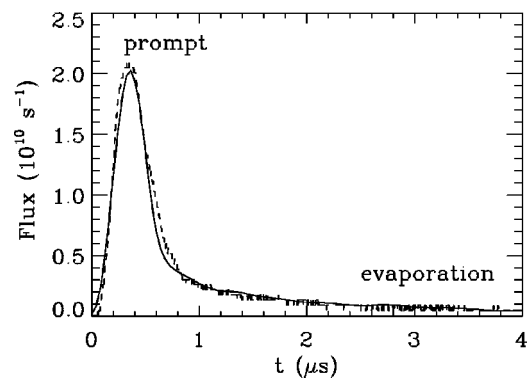


FIG. 3. The calculated (solid line) and measured (Ref. 17) (dashed line) electron flux. The plasma has an initial temperature of 60 K and density of  $0.40 \times 10^9$  cm $^{-3}$ .

than the average temperature. This loss of electrons continues until the electric potential near the edge of the plasma becomes large compared to  $k_B T_e$ .

The plasma needs roughly 1–2  $\mu$ s before the temperature in the different parts of the plasma equilibrate. This is much longer than the time needed for the distribution in each section of the plasma to come into local thermal equilibrium, Fig. 1. Figure 2 shows that the electron temperature drops by 40 K during the first 2  $\mu$ s which is mainly due to the expansion of the ion cloud; there is a small amount of cooling due to the electron evaporation.

In Fig. 3, we show a comparison between the calculated and measured<sup>17</sup> electron flux during the early stages of the plasma expansion. The plasma is in an 18 mV/cm electric field to push electrons into the detector. The experimental measurements have been shifted in time by 200 ns (due to uncertainties of electron travel time within the detector; the shift is 1 tick mark) and rescaled in magnitude by 15% (due to uncertainties in overall normalization) in Fig. 3; both of these changes are within experimental uncertainty. The calculations have been convolved over a time of 120 ns (due to time resolution within the detector). This convolution of the calculated data introduced only small changes to the calculated curve (the convolution is 1/2 tick mark). The slow decay of signal between 1–4  $\mu$ s and the ratio of the number of prompt electrons to delayed electrons does not depend on our manipulations; the simulations are in wonderful agreement with the measurement. During the time shown in the figure, the electron temperature drops by roughly a factor of three and the average density drops by roughly an order of magnitude. Thus, the plasma parameters are changing substantially during this time. We compared electron flux for other cases and obtained a similar level of agreement. All of the electron flux measurements show a peak in escaping electron flux followed by a small amount of escape. The initial peak in the flux comes from the electrons that escape before sufficient space charge is present to bind them to the plasma. The later small amount of flux arises from the electrons that evaporate from the plasma. The good agreement between the measurement and the calculation shows that we have accurately represented the electron thermalization in the ultra-cold plasma.

## B. Isothermal fluid model

As seen in the previous section, the plasma reaches local thermal equilibrium on a time scale roughly given by the electron relaxation time. The time required for the electron temperature to equilibrate across most of the plasma is longer but still fast compared to the plasma expansion time. Thus, we have performed simulations using thermal equilibrium for the electrons as an assumption because this type of simulation runs a factor of 100 faster than the Monte Carlo simulation. The inputs to this simulation are not direct data from the  $t=0$  plasma conditions. We use the Monte Carlo simulation to propagate the plasma for 1–2  $\mu\text{s}$  and use data from the simulation to determine the number of electrons that promptly leave the plasma and how much energy they carry to determine the actual number of electrons and the total energy in the remaining plasma.

The ion potential energy,  $U$ , is only a function of radius and is given by the equations

$$\frac{1}{r} \frac{\partial^2}{\partial r^2} [rU(r)] = - \frac{e^2}{\epsilon_0} [n_i(r) - n_e(r)],$$

$$n_e(r) = \alpha \exp\left[\frac{U(r)}{k_B T_e}\right], \quad (10)$$

$$\alpha = N_e \int 4\pi r^2 \exp\left[\frac{U(r)}{k_B T_e}\right] dr,$$

where the second equation uses the assumption of thermal equilibrium for the electron part of the plasma and the last equation ensures that the number of electrons equals  $N_e$ . These equations must be solved self consistently. The algorithm uses the ion potential energy to compute the acceleration,  $a(r)$ , the acceleration is used to move the ion positions and velocities forward by  $\delta t$ , the new ion density and kinetic energy are used in Eq. (10) with conservation of total energy to solve for  $T_e$  and the electron density. Three body recombination and electron scattering from Rydberg atoms somewhat complicate the algorithm as described below.

There is both a fundamental and a practical problem in solving Eq. (10) for the potential energy,  $U(r)$ . The fundamental problem is that the potential energy function is proportional to  $1/r$  at large distances. This means the electron density has the asymptotic form  $a + b/r$  at finite temperatures. This problem is an artifact of the thermal approximation: the density of electrons outside the ion cloud is too low for thermal equilibrium to be reached. Thus, we take a pragmatic approach in solving this problem: we make the electron temperature position dependent. Outside of the ion cloud we have the electron temperature smoothly decrease to zero over a range of roughly the size of the ion cloud. The  $1/T_e$  is constant for  $r < r_0 = 4 \cdot \sqrt{\langle r^2 \rangle}$  and increases quadratically  $T_e^{-1} \cdot [1 + 0.02 \cdot (r/r_0 - 1)^2]$ . Although this is a very simplified treatment of the electron density, it only affects a small fraction of the electrons since the temperature is so small.

The practical problem of solving Eq. (10) is more difficult. The trouble is that the equation is nonlinear in a manner that causes instabilities in the solution. We solved this equa-

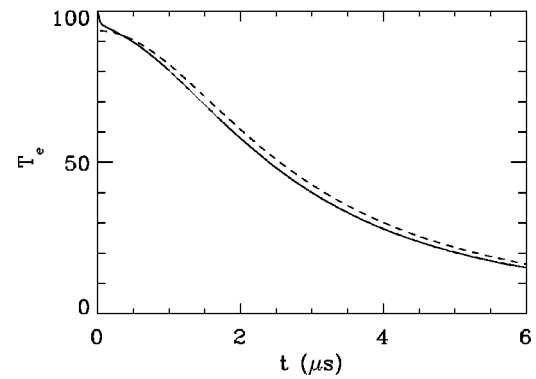


FIG. 4. The time dependence of the electron temperature using the Monte Carlo approximation (solid line) and the thermal approximation (dashed line). The plasma parameters are the same as Fig. 1.

tion using a technique similar to that discussed in Refs. 18–20. The details of this method are given in the Appendix.

## 1. Results

The simulations using the thermal approximation are roughly a factor 100 faster than those using the Monte Carlo approximation. Thus, it is important to test the accuracy of the thermal approximation. In Figs. 4 and 5, we compare properties for a plasma with initial values  $T_e = 100$  K and  $\bar{n}_e = 0.5 \times 10^9 \text{ cm}^{-3}$ . In Fig. 4, we compare the time dependence of the electron temperature for the Monte Carlo and thermal approximations over a time where the electron temperature drops by over a factor of 5. It is clear that the thermal approximation does a good job of reproducing the electron temperature over this time. In Fig. 5, we compare the position dependence of the weighted density for ions,  $r^2 n_i(r)$ , 1–3  $\mu\text{s}$  after the creation of the plasma. It is clear that the two approximations give very similar results. The differences arise because the temperature does not immediately become the same throughout the plasma but requires 1–2  $\mu\text{s}$  to equilibrate. The higher electron temperature at the center of the plasma causes the ions near the center to accelerate more than in the thermal approximation. As we lower the electron temperature or raise the density, the thermal approximation becomes better because the thermalization is

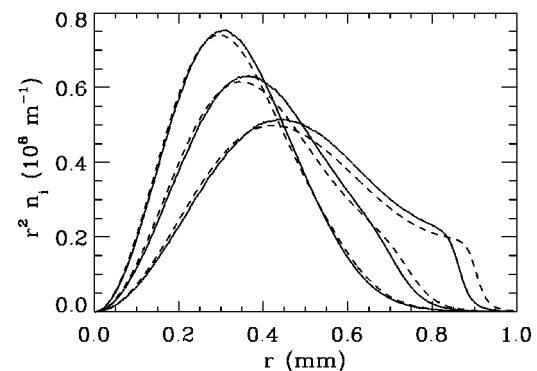


FIG. 5. The weighted ion density at 1, 2, and 3  $\mu\text{s}$  calculated using the Monte Carlo (solid line) and the thermal (dashed line) approximation. The plasma parameters are the same as Fig. 1.

much more rapid. The thermal and Monte Carlo approximations become almost indistinguishable if the electron temperature is lowered to 30 K at the density of Fig. 1.

### C. Rate equation model

The simplest level of approximation simplifies the thermal approximation even further. At low temperatures, the electron density and ion density must be approximately equal. We can use this idea to obtain an approximation for the electric potential:

$$n_e(r) = \alpha \exp\left[\frac{eV(r)}{k_b T_e}\right] \approx n_i(r). \quad (11)$$

This equation can be rearranged to give the approximation  $V(r) = (k_B T_e / e) \ln[n_i(r)] + \text{const}$ . If the ion density is proportional to a Gaussian, then the electric potential is a quadratic function of the distance from the center of the plasma,  $r$ , and the electric field strength is proportional to  $r$ . If the ions start with a Gaussian spatial distribution and zero velocity, the spatial distribution will remain a Gaussian if the acceleration is proportional to  $r$ .

At this level of approximation, the ion density is chosen to always have a Gaussian shape and the ion velocity linearly increases with distance from the center of the plasma:  $n_i(r, t) = N_i [\beta(t) / \pi]^{3/2} \exp[-\beta(t)r^2]$ ,  $v_i(r, t) = r\gamma(t)$ , and  $a_i(r, t) = r2\beta(t)k_B T_e(t) / M_i$ . Substituting this ansatz into the ion fluid equation gives the following ordinary differential equations:

$$\begin{aligned} \frac{d\gamma}{dt} + \gamma^2 &= 2k_b T_e(t)\beta(t) / M_i, \\ \beta(t) &= \beta(0) \exp\left[-2 \int_0^t \gamma(\bar{t}) d\bar{t}\right], \\ \frac{3}{2} k_B T_e(0) &= \frac{3}{2} k_B T_e(t) + \frac{3}{4} M_i \frac{\gamma^2(t)}{\beta(t)} + E_{\text{Ryd}}, \end{aligned} \quad (12)$$

where  $\gamma(0) = 0$  and the last relationship is from the conservation of energy: Thermal energy of electrons plus kinetic energy of the ions plus the energy in Rydberg atoms is constant. Simulations at this level of approximation are much faster than those carried out at the level of the thermal approximation. We use this approximation in searches for interesting plasma dynamics and for insight.

The errors at this level of approximation arise because the acceleration is not a linear function of  $r$  for all the ions. Also, some of the energy is carried away by electrons that escape the plasma at early times. Another error is because the conservation of energy equation does not include the electrostatic energy of the plasma. The relative size of these errors decreases as the electron temperature decreases. A final error arises because the three body recombination rate is proportional to  $n^3$  and thus recombination tends to lower the ion density at the center of the plasma; this error increases as the temperature decreases but is rarely large since only a few percent recombination occurs in the early stage of plasma evolution ( $< 20 \mu\text{s}$ ).

### IV. THREE BODY RECOMBINATION

Two electrons can interact with each other while in the neighborhood of a positive ion so that one of the electrons becomes bound to the ion and the other electron carries off the extra energy. The recombination rate increases like  $T_e^{-9/2}$  as the electron temperature decreases. At low temperatures, this becomes an extremely important process. We will describe in detail how we account for three body recombination in our model where we assume the electrons are in thermal equilibrium; a similar, but more complicated, treatment was followed for the Monte Carlo approximation.

We include three body recombination within our simulations by allowing for the possibility of a third species: Rydberg atoms. We assign the weight for a single Rydberg atom to be  $w_R$ . We chose the weight for Rydberg atom particles to be much less than the weight for ion particles:  $w_R \ll w_i$ . A typical value might be  $w_R = w_i / 16$ . By choosing the weight for Rydberg particles to be much less than that for ions, we reduce the fluctuation in the ion density and in the distribution of Rydberg states.

The rate for three body recombination into different bound states was taken from the simplified expression of Ref. 21; the recombination rate into a bound state with principle quantum number  $\nu$  is proportional to  $\nu^6$ . The recombination rate was taken to be

$$A_R = \frac{1 \text{ eV}}{k_B T_e} \nu^{*7} 2.8 \times 10^{-42} \frac{\text{m}^6}{\text{s}} \int n_e^2(r) n_i(r) 4\pi r^2 dr, \quad (13)$$

where  $\nu^* = \sqrt{13.6 \text{ eV} / 2k_B T_e}$  is the maximum principle quantum number for recombination. The number of Rydberg atoms formed during a time step is  $\delta t A_R$  and the number of Rydberg atom particles in the simulation was increased by  $\delta t A_R / w_R$ . Each Rydberg particle that was created was given a random initial position and velocity and binding energy. The principle quantum number was chosen to be

$$\nu = [y \cdot \nu^{*7} + (n_0 - 1/2)^7]^{1/7} - \frac{1}{2}, \quad (14)$$

where  $y$  is a random number with a flat distribution between 0 and 1 and  $n_0 = 6$  is not important since  $\nu^* \gg n_0$ ; this gives a probability proportional to  $(1/7)[(\nu + 1/2)^7 - (\nu - 1/2)^7] \approx \nu^6$  for the atom to be formed in state  $\nu$ . The radial position,  $r$ , of the Rydberg atom was chosen to be

$$y = \frac{\int_0^r n_e^2(\bar{r}) n_i(\bar{r}) \bar{r}^2 d\bar{r}}{\int_0^\infty n_e^2(\bar{r}) n_i(\bar{r}) \bar{r}^2 d\bar{r}}, \quad (15)$$

where  $y$  is a random number with a flat distribution between 0 and 1. The ion particle with position closest to that of the newly created Rydberg particle had its weight decreased by  $w_R$  and the number of electrons was also decreased. The radial velocity of the newly created Rydberg particle was set equal to that of the closest ion particle.

### V. PROCESSES INVOLVING RYDBERG ATOMS

The Rydberg atoms can play a large role in the low temperature plasmas; it is important to properly account for the processes involving Rydberg atoms. For the parameters

considered here, the evolution of Rydberg populations is controlled by electron-Rydberg scattering and by radiative decay.

### A. Electron-Rydberg scattering

Once a Rydberg atom is formed by three body recombination it can scatter electrons. The Rydberg atom can gain energy, lose energy or be re-ionized. We account for these processes using a Monte Carlo treatment of the collisions. We use the simple expressions in Ref. 9 to determine the rates for the different processes; we have checked the formulas of Ref. 9 for typical parameters present in our simulations and found them to be adequate.

The total de-excitation rate is given by

$$A_d = n_e(r) 7.2 \left( \frac{27.2 \text{ eV}}{k_b T_e} \right)^{0.17} \nu^{2.66} a_0^2 \alpha c, \quad (16)$$

and the total excitation rate is given by

$$A_e = n_e(r) 55 \left( \frac{k_b T_e}{27.2 \text{ eV}} \right)^{0.83} \nu^{4.66} a_0^2 \alpha c, \quad (17)$$

where  $a_0$  is the Bohr length,  $c$  is the speed of light,  $\nu = \sqrt{-13.6 \text{ eV}/E_R}$  is the principle quantum number of a Rydberg atom with internal energy  $E_R$ , and  $\alpha$  is the fine structure constant. The total collision probability during a time step is  $(A_d + A_e) \cdot \delta t$ .

For each Rydberg particle, the collision probability is computed at each time step and compared to a random number with a flat distribution between 0 and 1. If the random number is less than the collision probability, then a collision occurs and the energy of the Rydberg atom changes. The relative probability for excitation is  $f = 1/[1 - E_R/(3.83k_B T_e)]$  which decreases as the binding energy,  $-E_R$ , increases; note that the probability for excitation equals that for de-excitation when the binding energy is  $3.83k_B T_e$ . The change in energy for the Rydberg atom is

$$\begin{aligned} \Delta E_R &= E_R \cdot \left( \left[ \frac{1-f}{1-y} \right]^{0.2611} - 1 \right), \quad \text{if } y > f \\ &= -k_B T_e \ln \left( \frac{y}{f} \right), \quad \text{if } y < f, \end{aligned} \quad (18)$$

where  $y$  is a random number from a flat distribution between 0 and 1; note that the change in energy is positive if  $y < f$  and negative if  $y > f$ . The energy given to an electron when the atom is de-excited is proportional to the binding energy of the atom. Thus, more deeply bound atoms scatter less frequently but give larger amounts of energy to the plasma when the scattering does occur.

If the energy of the Rydberg atom is positive after the collision then ionization has occurred. That Rydberg particle is removed, the weight  $w_R$  is added back to the ion particle from which the Rydberg atom was originally formed, and weight is added to the electrons. In the vast majority of cases, this prescription puts the probability onto the nearest ion with the most similar speed because an atom is most

likely to be reionized just after it is formed; the probability for reionization decreases rapidly after a few collisions has driven the atom to lower states.

One assumption is that the energy given to the electron when the atom is scattered into more deeply bound states is shared by all the electrons. In reality, if the electron is given enough energy, it is more likely to escape the plasma while giving very little energy to the other electrons. This becomes more likely as the plasma expands because the electric field of the plasma decreases and more deeply bound Rydberg atoms are present at later times. We checked for the possible effects from this approximation by doing calculations at the two extremes. In one calculation, all of the energy was shared among all of the electrons and no electrons escaped. In the second calculation, any scattering that gave an electron 50% more energy than needed to escape the plasma was given to only one electron which was removed from the plasma without giving any energy to the remaining electrons. We found that this approximation had a small effect on the plasma dynamics.

### B. Radiative decay

We include the possibility for the Rydberg atoms to radiate a photon and decay into a lower energy state. Because the Rydberg atom is in an electron gas that rapidly mixes the angular momentum states of a  $\nu$  manifold, we use the expression for the decay rate from a state in the manifold  $\nu_i$  to  $\nu_f$ ,

$$A_{\nu_i \rightarrow \nu_f} = \frac{8\alpha^4 c}{3\sqrt{3}\pi a_0} \frac{1}{\nu_i^5 \nu_f} \frac{1}{1 - (\nu_f^2/\nu_i^2)}, \quad (19)$$

to compute the total radiative decay rate:

$$A_{\nu_i} = \sum_{\nu_f=\nu_0}^{\nu_i-1} A_{\nu_i \rightarrow \nu_f}, \quad (20)$$

where the lowest possible state that the atom can decay into  $\nu_0$ , is 3 or 4 (the exact value was not important).

At each time step, the total radiative decay probability,  $A_{\nu_i} \delta t$ , is compared to a random number with a flat distribution between 0 and 1. When the random number is less than the radiative decay probability, a photon is emitted. The final state,  $\nu_f$ , for the Rydberg atom is computed from

$$y = \sum_{\nu=\nu_0}^{\nu_f} A_{\nu_i \rightarrow \nu} / A_{\nu_i}, \quad (21)$$

where  $y$  is a random number with a flat distribution between 0 and 1. Atoms in state  $\nu_0$  do not scatter or decay further because they are the lowest energy states.

## VI. RESULTS

In this section, we present some of the new results relating to ultra-cold plasmas. Reference 12 contains earlier results on the role that three body recombination and electron-Rydberg scattering play in ultra-cold plasmas. Our simulations agreed with the measured expansion velocity of the plasma and with the trends in the distribution of Rydberg

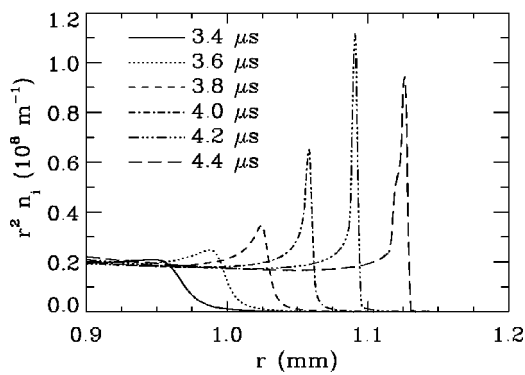


FIG. 6. The weighted ion density at 3.4 (solid line), 3.6 (dotted line), 3.8 (dashed line), 4.0 (dash-dotted line), 4.2 (dash-dot-dot line), and 4.4  $\mu$ s (long dashed line) calculated using the thermal approximation. This sequence shows the development of a spike in the ion density near 4.2  $\mu$ s. The plasma parameters are the same as Fig. 1.

binding energies. We also showed that the plasma was weakly coupled, even at low temperatures, due to the heating from three body recombination and electron-Rydberg scattering.

### A. Spike in ion density

A density spike forms in a plasma that expands into vacuum. The reason for this is clear in examining Fig. 1 of Ref. 12. The radial electric field increases with distance from the center of the plasma until near the edge; at large distances the electric field must decrease like  $1/r^2$ . There is a region near the plasma edge where the electric field decreases with  $r$  even though ions and electrons are present. In the region where the electric field is decreasing with increasing  $r$ , the ions at smaller  $r$  can catch up to ions at larger  $r$  and give rise to a density singularity when using fluid equations. In our treatment where ions are represented by particles that move according to Newton's equation, the density has a very large spike at this point. A similar spike was seen in the simulations of Ref. 8 for a non-neutral plasma.

In Fig. 6 we show the formation of this spike for a plasma with an initial temperature and average density of 100 K and  $10^9 \text{ cm}^{-3}$ . This figure gives a time sequence of the edge of the plasma showing how the spike forms. In Fig. 7, we show the density and the ion velocity as a function of position at  $t=4.6 \mu\text{s}$ . The density shows that just after the spike formation there are two spikes in the edge of the ion

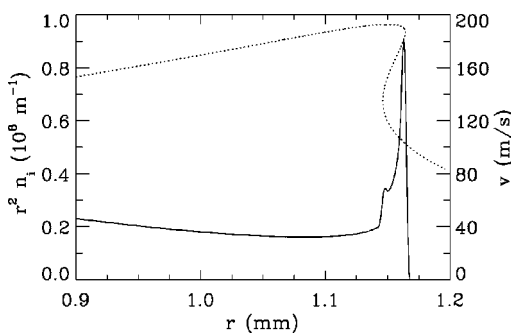


FIG. 7. The weighted ion density (solid line) and the ion velocity (dotted line) at 4.6  $\mu$ s. The plasma parameters are the same as Fig. 1.

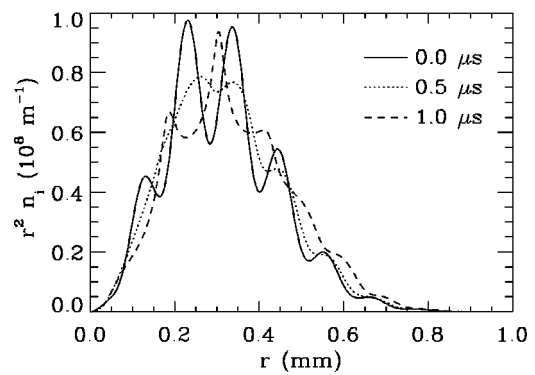


FIG. 8. The weighted ion density at 0.0 (solid line), 0.5 (dotted line), and 1.0  $\mu$ s (dashed line) calculated using the thermal approximation. This sequence shows 1/2 of the time sequence of an ion acoustic wave. There is an overall expansion which is why the peaks at 1.0  $\mu$ s do not exactly occur in the minima at 0.0.

plasma. The radial ion velocity as a function of position is shown as a dotted line. Note there are two positions where  $dv/dr$  diverges. While the spike is easily handled in the thermal approximation, the Monte Carlo approximation must be carefully checked because the electric field changes rapidly near the spike and can cause problems with energy conservation.

All of the ultra-cold plasmas formed a spike. The time required to form a spike depends most strongly on the electron temperature since the radial electric field is roughly proportional to  $T_e$ . There is a weaker dependence on the density since the number of electrons that escape the plasma depends on the number of ions. Finally, the time to spike formation depends on the size of the plasma since the electric field near the plasma edge is inversely proportional to the squared size of the plasma. The density spike is not as obvious in the electron density. Thus, an experimental measurement of the density spike may be more feasible if the ions are imaged.

### B. Ion acoustic waves

At the suggestion of Killian, we deliberately put a modulation on the ion density. Because our simulations assume spherical symmetry, we started the ions with a density  $n_i = \alpha \exp(-\beta r^2) \cdot [1 + a \cos(kr)]$  where  $\alpha$  is a normalization constant to give the correct number of ions,  $\beta$  limits the size of the plasma, and the term in square brackets modulates the Gaussian. Although this exact type of modulation cannot be realized experimentally, it can give insight into how a density modulation of an ultra-cold plasma might behave.

In Fig. 8, we show the ion density at three times when  $T_e = 100 \text{ K}$ ,  $N_i = 3.37 \times 10^5$ ,  $\beta = 1.5/(340 \mu\text{m})^2$ , the modulation amplitude  $a = 0.2$ , and the modulation wave number is  $k = 6\pi/340 \mu\text{m}$ . The sequence of frames shows that the modulation has a wave type behavior on top of the expansion of the plasma. This is an ion acoustic wave modified by the expansion of the plasma. An ion acoustic wave has a frequency  $\omega = k \sqrt{k_B T_e / M_i}$  which gives a period of roughly 1.4  $\mu$ s for the parameters in Fig. 8; this estimate of the period is somewhat smaller than the period from the simulation because both  $k$  and  $T_e$  are decreasing. The simulations were

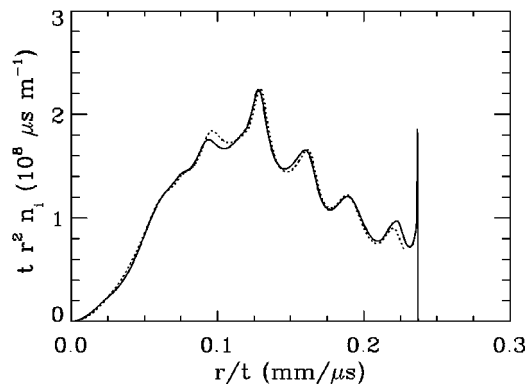


FIG. 9. The scaled weighted ion density at 10.0 (solid line) and 12.0  $\mu\text{s}$  (dotted line) calculated using the thermal approximation. This sequence shows how the ion acoustic wave gets frozen into the expanding ion density.

carried out using both the thermal and Monte Carlo approximations and gave very similar results; thus, the ion acoustic waves do not damp rapidly because of electron scattering and fluctuations.

Ion acoustic waves have an interesting property in these ultra-cold plasmas. The frequency decreases with the square root of the electron temperature and is proportional to the reciprocal of the wavelength. Once the plasma starts expanding, all lengths increase roughly linear with time. Also, the electron temperature decreases as the plasma expands. Since the frequency is decreasing faster than  $1/t$ , the modulations of the plasma tend to get frozen into the expansion. This can be seen in Fig. 9 where we show the ion density at two times but compensated for the expansion; the modulation of the ion density has hardly changed except for an overall expansion. It seems that it should be possible to experimentally measure these effects.

### C. Distribution of Rydberg states

In Ref. 12, we speculated that the distribution of Rydberg states could be linked to the radial speed of the Rydberg atom because the Rydberg atom has the speed of the positive ion at the time the recombination occurs. Thus, Rydberg atoms formed early in the plasma expansion would have lower speed and larger binding energy of the electron to the positive ion than atoms formed later in the plasma expansion. In Fig. 10, we show the distribution of binding energies for a plasma with an initial electron temperature of 66 K and average density of  $0.5 \times 10^9 \text{ cm}^{-3}$  for two different radial velocities. It is clear that the faster atoms are less strongly bound, as suggested in Ref. 12.

We had also suggested that electron-Rydberg scattering was responsible for some of the peculiar distribution of Rydberg atoms observed in Fig. 2(b) of Ref. 4; this figure showed that the lower temperature plasma had more deeply bound Rydberg atoms. This contradicts the expectation that higher temperature plasma leads to larger binding energies. In Fig. 11, we show the distribution of Rydberg atoms for two different temperatures and an initial average density of  $0.5 \times 10^9 \text{ cm}^{-3}$  which are the parameters in Fig. 2 of Ref. 4. It is clear that very similar trends in the binding energy are

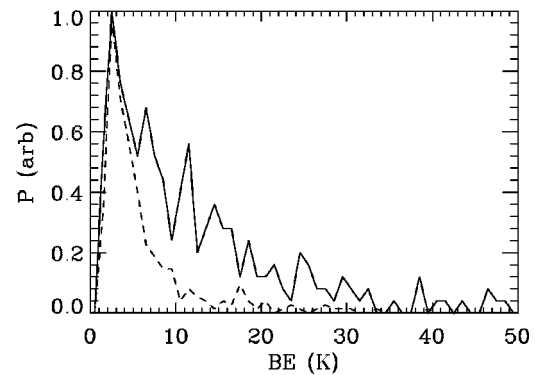


FIG. 10. The binding energy distribution of electrons to positive ions for atoms with radial velocities of roughly 8 m/s (solid line) and 32 m/s (dashed line). Slower atoms tend to have larger binding energies.

observed. The lower temperature plasmas give the atoms with the largest binding energy because the lower temperature plasma has more atoms formed at early times and because the lower temperature plasma does not expand as quickly as the high temperature plasma; both of these effects tend to give more deeply bound atoms because it gives more time for electron-Rydberg scattering. This validates our earlier suggestion.

A more problematic and curious result was presented as the inset to Fig. 3 of Ref. 4. This figure showed that a plasma with an initial temperature of  $\sim 6 \text{ K}$  and a density of  $10^{10} \text{ cm}^{-3}$  had a population of Rydberg atoms with a strange time dependence: The population initially decreased before increasing at later times. This seems to be in conflict with three body recombination as the mechanism for formation of Rydberg atoms because the number of Rydberg atoms should only increase with time. However, our simulations for similar parameters give results with the same behavior. In Fig. 12, we show the number of Rydberg atoms that *could have been detected* with the apparatus of Ref. 4 as a function of time; these are states with a principle quantum number greater than 40. In our simulations, the number of atoms formed does increase with time but the number of atoms that could have been detected initially decreases before increasing at later times. The decrease in the number of detectable

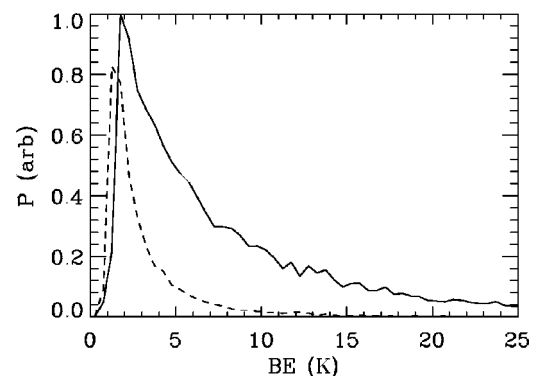


FIG. 11. The binding energy distribution of Rydberg atoms 50  $\mu\text{s}$  after plasma creation for 66 K (solid line) and 133 K (dashed line) initial temperatures. The lower temperature plasma has the more deeply bound atoms because the lower temperature plasma expands more slowly.

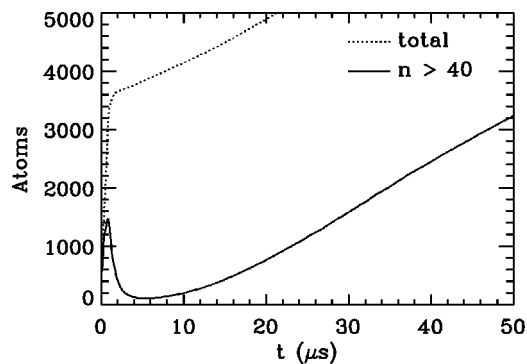


FIG. 12. The number of Rydberg atoms above the  $\nu=40$  state (solid line) and the total number of atoms (dotted line). Rydberg atoms above  $\nu=40$  could be detected with the apparatus of Ref. 4. The total number of atoms only increases with time. The plasma is initially at a temperature of 10 K and an average density of  $10^9 \text{ cm}^{-3}$ .

atoms is the result of two effects: (1) The plasma heats at early times (because the large number of three body recombinations and electron-Rydberg atom scattering is more important than adiabatic cooling) which slows the three body recombination rate *and* reduces the range of atoms that can be detected (atoms with binding energy less than  $2k_B T_e$  are typically ionized and principle quantum number of 40 corresponds to a binding energy of roughly 100 K). (2) The electron-Rydberg scattering causes atoms (initially at detectable binding energies) to scatter into states too deeply bound to be detected. At later times the number of detectable atoms increases because the temperature and the density decrease as the plasma expands.

#### D. Rydberg gas to plasma conversion

As a final system, we attempted to simulate the Virginia–Aime Cotton experiments<sup>5</sup> where a gas of cold Rb or Cs atoms were excited into Rydberg states; the Rydberg states have low angular momentum and are not mixed with the degenerate manifold of hydrogen like states. The cold gas of Rydberg atoms converted into an ultra-cold plasma in 1–10  $\mu\text{s}$ ; the time needed for conversion depended on the density of Rydberg atoms, the binding energy of the Rydberg atoms, and the presence of a small population of hot  $\sim 300$  K Rydberg atoms.

From the experiments it seems that the small population of hot Rydberg atoms leads to a small amount of ionization due to Rydberg–Rydberg collisions. This gives a small linear rate for number of free electrons. The electrons escape the region of the Rydberg gas until a space charge builds up that is sufficient to bind subsequent electrons. Shortly after the electrons become bound to the space charge, the Rydberg gas converts to a plasma in a couple microseconds. The surprising part of the measurement is the inset of Fig. 1. This shows that while the Rydberg gas is being converted into a plasma there are only two populations: Rydberg atoms in the initial, low angular momentum state and free electrons.

We simulated the conversion of a Rydberg gas into a plasma using known atomic processes. In our simulations, the Rydberg gas converted into a plasma on roughly the time

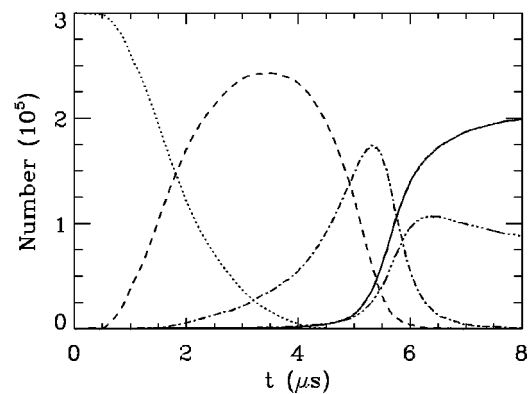


FIG. 13. The populations in various types of states in an initial Rydberg gas of Rb atoms. The dotted line is the low angular momentum initial states and states that would have been indistinguishable from the initial state in Ref. 5. The dashed line is high angular momentum states in the nearest 2 principle quantum number. The dot–dashed line is for other high angular momentum states that could be detected. The dot–dot–dot–dash line are states that are too deeply bound to be detected. The solid line is the free electrons. The initial state was the  $36d$  state, there were  $3 \times 10^5$  Rydberg atoms, and the Rydberg gas is a cylinder with an axis 1.2 mm long and radius of 0.1 mm. All simulations showed a substantial population of high angular momentum states before a substantial formation of free electrons which does not agree with measurements.

scale seen in the experiments. However, we found that our best estimates of atomic collisions always gave a substantial population of atoms in high angular momentum, hydrogen-like states. As an example, we show the evolution of populations in one of our simulations in Fig. 13. In this simulation, we include (1) the electron cross sections from the initial state into nearby states by treating the Rydberg atom as a quantum system but the scattering electron as a classical particle moving on a straight line, (2) the electron scattering from hydrogen like states of the Rydberg atom by performing calculations where both electrons are classical particles and the electrons on the atom are completely mixed in orientation and phase, (3) electron–electron collisions to give thermalization of the free electrons, (4) the hot Rydberg atom–cold Rydberg atom cross section by a simple estimate of 10 times geometrical, (5) the escape of electrons with energy higher than the binding energy of the space charge, and (6) photon emission from Rydberg states.

The simulations have the Rydberg gas convert into a plasma on roughly the time scales seen in the experiment. The conversion seems to happen by free electrons scattering the initial state into nearby high angular momentum states. Free electrons scattering from these states sometimes cause transitions to more deeply bound states which adds energy to the electrons or to less deeply bound states which removes energy from the electrons. After many collisions roughly 3/4 of the initial atoms are ionized and 1/4 have dropped into (relatively) deeply bound states.

All of the simulations give behavior not seen in the experiment. Namely, a substantial population of high angular momentum states appears before a substantial population of free electrons. The population of high angular momentum states should have been detectable in Ref. 5. The reason for the large population of high angular momentum states is based on a general feature of electron-Rydberg scattering and

will not change even if the details of our simulation are wrong: electron-Rydberg scattering is strongest for dipole allowed transitions with small energy changes. Thus, the largest cross section, by far, is the scattering from low angular momentum states into high angular momentum states at nearby energies. Only after many scatterings of electrons on Rydberg atoms does ionization occur.

Our simulations assumed that it is only the free electrons that cause transitions in the atoms. We simulated other scattering processes and found that none of them were within 2 orders of magnitude of transitions caused by electrons. The free electrons have roughly the same speed as the weakly bound electron of the Rydberg atom and are charged; transition rates are at their peak in this case. All other transitions would be caused by uncharged objects with speeds several orders of magnitude smaller than the electron speed. We computed or estimated: (1) the collision rate between an atom in a high angular momentum state and an atom in the initial state, (2) the collision rate between two atoms in high angular momentum states, (3) the possibility that inhomogeneous electric fields accelerate the atoms with high angular momentum, and (4) the time for two atoms (in any combination of high and low angular momentum) to become attracted through long range electric forces to small enough distances to ionize. Basically, there are 4 objects in the plasma: low angular momentum Rydberg atoms, high angular momentum Rydberg atoms, electrons, and inhomogeneous electric fields. We simulated the pair wise interaction of all of them and found that only electrons cause substantial transitions and ionization.

The mechanism for the conversion of the Rydberg gas in Ref. 5 into a plasma is still unknown.

## VII. CONCLUSIONS

We have simulated the expansion of ultra-cold plasmas at several levels of approximation. We have presented the details and some of the results of our simulations. We find that the ultra-cold plasmas present an interesting interplay between atomic and plasma processes. The initial energy available to the electrons can be controlled by tuning the frequency of the laser that ionizes the cold atomic gas. However, the plasma rapidly heats at very low temperatures due to three body recombination and subsequent electron-Rydberg collisions. We find that our simulations reproduce all of the features of published experiments<sup>2-4</sup> when a plasma is directly created. Our simulations of the conversion of a Rydberg gas into a plasma do not agree with the measured time dependence of the populations.<sup>5</sup>

We have presented the results of simulations that show how some plasma phenomena (e.g., ion acoustic waves, spikes, electron thermalization, ...) are manifested in ultra-cold plasmas. We find that the plasma expansion does not destroy the ion acoustic waves; we also find that the plasma expansion tends to freeze in an ion acoustic wave. We find that a spike in the ion density forms on a time scale  $\sim 10 \mu\text{s}$  and persists for times longer than  $100 \mu\text{s}$ . We find that the distribution of binding energies of the Rydberg atoms is correlated with the radial velocity of the Rydberg atom. We find

that the electron component of the ultra-cold plasma does not form a strongly coupled plasma for times less than  $100 \mu\text{s}$  for initial electron temperatures less than 150 K and densities less than  $2 \times 10^9 \text{ cm}^{-3}$ .

## ACKNOWLEDGMENTS

We gratefully acknowledge conversations with M. S. Pindzola, S. L. Rolston, J. Roberts, T. C. Killian, T. F. Gallagher, P. Gould, E. Eyler, S. Mazevet, and G. Raithel. We also thank J. Roberts and S. L. Rolston for providing us with the experimental data shown in Fig. 3 before publication.

This work was supported by the Chemical Sciences, Geosciences, and Biosciences Division of the Office of Basic Energy Sciences, U.S. Department of Energy.

## APPENDIX: NUMERICAL SOLUTION OF SELF CONSISTENT EQUATIONS

The solution of the self consistent equations, Eqs. (10), is computationally challenging. The method we used is an iterative technique. Assume that we have a solution,  $U_0(r)$ , which is close to the exact solution of Eq. (10). The exact solution can be expressed as the sum of the approximate solution and a small change,  $U(r) = U_0(r) + \delta U(r)$ . If we only keep first order terms in  $\delta U$ , the electron density has the form

$$n_e(r) = \left( 1 + \eta + \frac{\delta U(r)}{k_B T_e} \right) n_{e,0}(r), \quad (\text{A1})$$

where  $n_{e,0}$  is the electron density that gives the potential  $U_0$  and the constant  $\eta$  gives the correct normalization for the density:

$$\eta = - \frac{1}{N_e} \int_0^\infty 4\pi r^2 \frac{\delta U(r)}{k_B T_e} n_{e,0}(r) dr. \quad (\text{A2})$$

The change in the potential is given by  $\delta U = \delta U_1 - \eta \delta U_2$  where the  $\delta U_{1,2}$  are solutions of the inhomogeneous equations,

$$\begin{aligned} \mathcal{L}\delta U_1 &= - \frac{e^2}{\epsilon_0} [n_i(r) - n_{e,0}(r)] - \frac{1}{r} \frac{\partial^2}{\partial r^2} r U_0(r), \\ \mathcal{L}\delta U_2 &= - \frac{e^2}{\epsilon_0} [n_i(r) - n_{e,0}(r)], \end{aligned} \quad (\text{A3})$$

where the differential operator

$$\mathcal{L} = \frac{1}{r} \frac{\partial^2}{\partial r^2} r - \frac{e^2}{\epsilon_0 k_B T_e} n_{e,0}(r). \quad (\text{A4})$$

The inhomogeneous functions  $\delta U_{1,2}$  go to 0 as  $r \rightarrow \infty$ . The solution,  $U$ , is obtained by iteration. Because ion density is obtained from low order basis functions, there is no point in a high-order approximation for  $\mathcal{L}$ . We use the three-point difference

$$\frac{1}{r} \frac{\partial^2}{\partial r^2} r U = \frac{r_{j+1} U_{j+1} - 2r_j U_j + r_{j-1} U_{j-1}}{r_j \delta r^2}, \quad j \neq 0,$$

$$\frac{1}{r} \frac{\partial^2}{\partial r^2} r U = 3 \frac{U_1 - 2U_0 + U_1}{\delta r^2}, \quad j=0, \quad (\text{A5})$$

where the special case at  $j=0$  is found by noting that  $U$  only has even powers of  $r$ .

This iterative scheme only works when the initial  $U_0$  is close to the exact  $U$ . The initial guess for  $U_0$  at time  $t$  is obtained by extrapolating the electron density from previous time steps. The first guess for  $U_0$  at the starting time  $t=0$  is obtained by relaxation.

At the initial time, the number of electrons and ions, the total energy of the plasma, and the spatial dependence of the ion density is determined. The algorithm for evolving the plasma proceeds in three steps. In the first step, the electron and ion densities are used to compute the electric field which determines the acceleration of the ions; the ion positions and velocities are then stepped forward one time step,  $\delta t$ . In the second step, the electron temperature and density are iterated until Eq. (10) is satisfied and the total energy is conserved; both the electron thermal energy and the electrostatic energy depend on the temperature. In the third step, the electron scattering from any Rydberg atoms and the three body recombinations are computed. The electron scattering from Rydberg atoms tends to de-excite the atoms and heat the electrons.

- <sup>1</sup>H. Metcalf and P. van der Straten, *Laser Cooling and Trapping* (Springer-Verlag, New York, 1999).
- <sup>2</sup>T. C. Killian, S. Kulin, S. D. Bergeson *et al.*, Phys. Rev. Lett. **83**, 4776 (1999).
- <sup>3</sup>S. Kulin, T. Killian, S. Bergeson, and S. Rolston, Phys. Rev. Lett. **85**, 318 (2000).
- <sup>4</sup>T. Killian, M. J. Lim, S. Kulin *et al.*, Phys. Rev. Lett. **86**, 3759 (2001).
- <sup>5</sup>M. Robinson, B. Laburthe Tolra, M. W. Noel *et al.*, Phys. Rev. Lett. **85**, 4466 (2000).
- <sup>6</sup>E. Elyer *et al.*, Bull. Am. Phys. Soc. **45**, 56 (2000).
- <sup>7</sup>S. Dutta, D. Feldbaum, A. Walz-Flannigan *et al.*, Phys. Rev. Lett. **86**, 3993 (2001).
- <sup>8</sup>D. Feldbaum, N. Morrow, S. Dutta, and G. Raithel, Phys. Rev. Lett. **89**, 173004 (2002).
- <sup>9</sup>P. Mansbach and J. Keck, Phys. Rev. **181**, 275 (1969).
- <sup>10</sup>A. N. Tkachev and S. I. Yakovlenko, Laser Phys. **9**, 977 (2001).
- <sup>11</sup>S. Mazevet, L. A. Collins, and J. D. Kress, Phys. Rev. Lett. **88**, 055001 (2002).
- <sup>12</sup>F. Robicheaux and J. D. Hanson, Phys. Rev. Lett. **88**, 055002 (2002).
- <sup>13</sup>S. G. Kuzmin and T. M. O'Neil, Phys. Rev. Lett. **88**, 065003 (2002).
- <sup>14</sup>S. G. Kuzmin and T. M. O'Neil, Phys. Plasmas **9**, 3743 (2002).
- <sup>15</sup>M. S. Murillo, Phys. Rev. Lett. **87**, 115003 (2001).
- <sup>16</sup>G. Schmidt, *Physics of High Temperature Plasmas* (Academic, New York, 1979).
- <sup>17</sup>J. Roberts and S. Rolston (private communication, 2002).
- <sup>18</sup>C. Sack and H. Schamel, Phys. Rep. **156**, 311 (1987).
- <sup>19</sup>R. L. Dewar and E. Valeo, *Proceedings of the 6th Conference on Numerical Simulations of Plasmas*, held at Lawrence Berkeley Laboratory, University of California/Berkeley, California, 1973.
- <sup>20</sup>D. W. Forslund *et al.*, *Proceedings of the 7th Conference on Numerical Simulations of Plasmas*, held at Courant Institute, New York University, 1975.
- <sup>21</sup>M. Pajek and R. Shuch, Hyperfine Interact. **108**, 185 (1997).